Suppressor screen connects HAD protein function to metabolic control in *Plasmodium falciparum*

Ann M. Guggisberg [1]
Aakash Y. Gandhi [1]*
Samuel J. Erlinger [1]#
Emilio F. Merino [2]
Maria B. Cassera [2]
Audrey R. Odom John [1,3]

[1] Department of Pediatrics, Washington University School of Medicine, St. Louis, Missouri, 63110, USA
[2] Department of Biochemistry and Molecular Biology, and Center for Tropical and Emerging Global Diseases (CTEGD), University of Georgia, Athens, GA 30602, USA
[3] Department of Molecular Microbiology, Washington University School of Medicine, St. Louis, Missouri, 63110, USA

Current affiliations:
* Medical Scientist Training Program, University of Texas Southwestern Medical Center, Dallas, Texas, 75235, USA
# Medical Scientist Training Program, Johns Hopkins University, Baltimore, Maryland, 21205, USA

Corresponding author:
Audrey R. Odom John
aodom@wustl.edu

Abstract

In the malaria parasite *Plasmodium falciparum*, isoprenoid synthesis from glycolytic intermediates is essential for survival. The antibiotic and antimalarial fosmidomycin (FSM) inhibits isoprenoid synthesis. In FSM-resistant *P. falciparum*, we identify a loss-of-function mutation in *HAD2* as causative for resistance. Enzymatic characterization shows that HAD2, a member of the haloacid dehalogenase-like hydrolase (HAD) superfamily, functions as a nucleotidase. Harnessing a growth defect in *HAD2*-mutant parasites, we select for suppression of HAD2-mediated FSM resistance and uncover hypomorphic suppressor mutations in the locus encoding the glycolytic enzyme phosphofructokinase. Metabolic profiling demonstrates that

FSM resistance is achieved via increased steady-state levels of MEP pathway and glycolytic intermediates and confirms reduced PFK9 function in the suppressed strains. We identify HAD2 as a novel regulator of malaria glycolytic metabolism and drug sensitivity. Our study informs the biological functions of an evolutionarily conserved family of metabolic regulators and reveal a previously undescribed strategy for cellular glycolytic regulation.

Keywords: Plasmodium, malaria, isoprenoid, resistance, fosmidomycin, suppressor, glycolysis, metabolism, regulation

Introduction

As an obligate intracellular parasite of human erythrocytes, the malaria parasite *Plasmodium falciparum* has unique metabolic features that may be exploited to discover new drug targets and develop new therapies. In the red blood cell niche, *Plasmodium* parasites depend on glucose metabolism. Infection with *Plasmodium* spp. results in a nearly 100-fold increase in glucose import in red blood cells (Mehta, Sonawat, & Sharma, 2006; E. Roth, 1990; E. F. Roth, 1987). Despite these energy requirements, the parasite demonstrates little aerobic respiration via the TCA cycle. Instead, it relies on anaerobic glycolysis to produce ATP (Bowman, Grant, Kermack, & Ogston, 1961; Krungkrai, Burat, Kudan, Krungkrai, & Prapunwattana, 1999; MacRae et al., 2013; Scheibel & Miller, 1969).

Besides ATP production, glucose also has a number of anabolic fates in *P. falciparum*. One such fate is the synthesis of isoprenoids. Isoprenoids are a large class of hydrocarbons with extensive structural and functional diversity (Gershenzon & Dudareva, 2007). In the malaria parasite,

61 isoprenoids perform several essential functions, including protein prenylation, dolichylation, and
62 synthesis of GPI anchors (Guggisberg, Amthor, & Odom, 2014; Imlay & Odom, 2014; Jordão,
63 Kimura, & Katzin, 2011). Recently, *P. falciparum* isoprenoid intermediates have also been
64 implicated in modulation of vector feeding behavior (Emami et al., 2017).
65
66 Despite this diversity, all isoprenoids are synthesized from a common five-carbon building block,
67 isopentyl pyrophosphate (IPP). Evolution has produced two distinct routes for IPP synthesis: the
68 mevalonate pathway, found in archaea, fungi, animals, and the cytoplasm of plants; and the
69 methylerythritol phosphate (MEP) pathway, found in most eubacteria, plant chloroplasts, and
70 apicomplexan parasites such as *P. falciparum* (Lange, Rujan, Martin, & Croteau, 2000). Because
71 of its absence in the human host, the MEP pathway is a compelling target for antimalarial
72 development. The antibiotic and antimalarial fosmidomycin (FSM) is a competitive inhibitor of
73 the first committed enzymatic step of the MEP pathway, catalyzed by 1-deoxy-D-xylulose-5-
74 phosphate reductoisomerase (DXR, E.C. 1.1.1.267) (Koppisch, Fox, Blagg, & Poulter, 2002;
75 Kuzuyama, Shimizu, Takahashi, & Seto, 1998; Steinbacher et al., 2003). FSM has been validated
76 as a specific inhibitor of the MEP pathway in *P. falciparum* (Zhang et al., 2011) and is a valuable
77 chemical tool to study MEP pathway biology and essential metabolism in the parasite.
78
79 Parasites are likely to control the proportion of glucose used for energy production versus
80 production of secondary metabolites, such as isoprenoids. We previously used a screen for FSM
81 resistance to identify HAD1, a metabolic regulator whose loss results in increased levels of MEP
82 pathway intermediates and resistance to MEP pathway inhibition. HAD1 is a cytoplasmic sugar
83 phosphatase that can dephosphorylate glycolytic intermediates upstream of the MEP pathway

84 (Guggisberg, Park, et al., 2014). HAD1 belongs to the haloacid dehalogenase-like hydrolase
85 (HAD) enzyme superfamily (Interpro domain IPR023214) and more specifically, the IIB
86 (IPR006379) and Cof-like hydrolase (IPR000150) subfamilies (Hunter et al., 2012). While
87 HADs are found in all kingdoms of life, HAD1 is most related to bacterial members of this
88 superfamily (Guggisberg, Park, et al., 2014; Kuznetsova et al., 2006), and is implicated in
89 metabolic regulation, stress response, and phosphate homeostasis (M. J. Kang et al., 2005; Y.
90 Kang, Weber, Qiu, Kiley, & Blattner, 2005; Pratish & Radhakrishnan, 2014; Roberts, Lee,
91 McCullagh, Silversmith, & Wemmer, 2005; Sun & Vanderpool, 2013). However, many
92 members of this superfamily remain uncharacterized. The study of HAD proteins in
93 evolutionarily and metabolically distinct organisms such as *P. falciparum* will greatly facilitate
94 our understanding of this ubiquitous class of enzymes.
95
96 In this study, we describe the discovery of HAD2, a second HAD family member in *P.*
97 *falciparum*. We find that HAD2 is required for metabolic homeostasis and normal asexual
98 replication in malaria parasites. Loss of HAD2 dysregulates glycolysis and misroutes metabolites
99 towards the MEP pathway, leading to drug resistance. In vitro, HAD2 dephosphorylates
100 nucleotides. Selection for suppression of drug resistance identifies mutations in *PFK9*, which
101 encodes the canonical glycolytic regulatory enzyme, phosphofructokinase. Through our forward
102 genetics approach, we further define the biological role of the HAD protein superfamily and
103 uncover a novel mechanism of regulation of cellular central carbon metabolism and drug
104 sensitivity.
105
106

107 # Results

108

109 ## A nonsense allele of *HAD2*, homolog of the MEP pathway regulator HAD1, in

110 ## FSM^{R} strain E2

111 The MEP pathway is responsible for the synthesis of the essential isoprenoid precursors IPP and

112 DMAPP. This pathway is specifically inhibited by the antibiotic fosmidomycin (FSM)

113 (Gisselberg, Dellibovi-Ragheb, Matthews, Bosch, & Prigge, 2013; Yeh & DeRisi, 2011; Zhang

114 et al., 2011). We previously generated *P. falciparum* strains resistant to FSM. Mutations in

115 HAD1 (PF3D7_1033400) cause the resistance phenotype in a majority of these strains

116 (Guggisberg, Park, et al., 2014). However, strain E2 remained uncharacterized. We find that E2

117 is less sensitive to FSM than its parental line (Figure 1A), as previously reported (Guggisberg,

118 Park, et al., 2014). This resistance phenotype is not due to changes in the *HAD1* locus or changes

119 in *DXS*, *DXR*, or *HAD1* expression (Figure 1-figure supplement 1). To identify genetic changes

120 that may result in FSM resistance, we performed whole genome sequencing (and identified the

121 A469T mutation in PF3D7_1226300 (PlasmoDB ID), hereafter referred to as *HAD2*

122 (Aurrecoechea et al., 2009). Whole genome sequencing data has been deposited in the NCBI

123 BioProject and Sequence Read Archive databases (Guggisberg, Kelly, Hodge, & Odom, 2013a,

124 2013b). Sanger sequencing of the *HAD2* locus in strain E2 confirmed the presence of the A469T

125 allele. This allele encodes a truncated R157X variant and therefore we expect HAD2 function is

126 lost in strain E2.

127

128

129 Interestingly, HAD2 is a close homolog of the known MEP pathway regulator, the sugar
130 phosphatase HAD1 (Guggisberg, Park, et al., 2014). Sequence homology places both proteins in
131 the haloacid dehalogenase-like hydrolase (HAD) superfamily and further within the IIB and Cof-
132 like hydrolase subfamilies (Interpro IPR006379 and IPR000150, respectively) (Hunter et al.,
133 2012). While no structural information exists for *P. falciparum* HAD2, the structure of the
134 *Plasmodium vivax* HAD2 (PVX_123945, PvHAD2) has been solved (PDB ID 2B30). PvHAD2
135 (93% identical and 98% similar to PfHAD2) possesses the structural motifs found in other HADs,
136 including a core and cap domain (Figure 1B). HAD2 and HAD1 protein sequences share ~29%
137 sequence identity and ~53% sequence similarity, and HAD2 possesses the four conserved
138 sequence motifs found in HAD proteins (Figure 1C). We hypothesized that HAD2, like HAD1,
139 regulates metabolism in *P. falciparum*.
140

141 **HAD2 is a nucleotidase**

142 Based on sequence homology to HAD1 and other HAD proteins, we predicted that HAD2 would
143 function enzymatically as a phosphatase. The phosphatase activity of purified recombinant
144 HAD2 was confirmed using *para*-nitrophenyl phosphate (*p*NPP), a chromogenic phospho-
145 substrate (Kuznetsova et al., 2005, 2006) (specific activity, 1.05 ± 0.22 μmol product/min/mg
146 enzyme). Since recent work on the HAD2 homolog from *P. vivax* (PvHAD2) suggested
147 promiscuous substrate recognition, including sugar phosphates and nucleotides (Srinivasan,
148 Kempaiah Nagappa, Shukla, & Balaram, 2015), we determined the substrate specificity of
149 HAD2. Surprisingly, we find markedly weaker activity against sugar phosphate substrates than
150 by HAD1 and its PvHAD2 homolog (Guggisberg, Park, et al., 2014; Srinivasan et al., 2015). In

151 contrast, we find that HAD2 robustly utilizes several nucleotide substrates (Figure 2). Kinetic
152 parameters for HAD2 against its top five substrates are found in Table 1.
153
154 We hypothesized that loss of HAD2-mediated nucleotidase function in FSM^R strain E2 might
155 result in changes in cellular nucleotide levels. We evaluated nucleotide levels using a recently
156 described liquid chromatography-mass spectrometry (LC-MS) method (Laourdakis, Merino,
157 Neilson, & Cassera, 2014). Total steady-state levels of several nucleotides are not altered in
158 strains lacking functional HAD2 (Figure 2-figure supplement 1).
159

160 Growth defect of *had2*^{R157X} parasites drives loss of FSM resistance

161 FSM^R *had2*^{R157X} parasites are growth-attenuated compared to the parental parasite strain (Figure
162 3, purple vs. black line), a phenotype that is reversed following prolonged culture without FSM.
163 Importantly, we find that improved growth rates also correlate with restored FSM sensitivity. We
164 hypothesized that in FSM^R *had2*^{R157X} parasites, FSM resistance due to loss of HAD2 resulted in a
165 fitness cost. Over time, the FSM^S population would thus predominate. To test this possibility, we
166 selected five clones derived from E2 by limiting dilution in the absence of drug pressure (Figure
167 4). Three of the five clones were found to be FSM^R (designated clones E2-R1, -R2, and -R3),
168 and two were FSM^S (designated E2-S1 and -S2) (Figure 4). Notably, the FSM^S clones were no
169 longer growth impaired (Figure 3, teal vs. purple line). To our surprise, all five E2 clones had
170 maintained loss of HAD2 via the *had2*^{R157X} mutation.
171

172 Long-term culture selects for hypomorphic suppressor mutations in *PFK9*

173 We hypothesized that these FSM^S E2 clones, driven by a fitness advantage, had acquired new
174 suppressor mutation(s) at an additional locus, resulting in loss of FSM resistance and an increase
175 in growth rate. We performed whole genome sequencing on the five E2 clones to identify any
176 genetic changes that segregated with the FSM^R and FSM^S (suppressed) phenotypes. Indeed, we
177 find that a mutation (*pfk9*^{T1206I}) in the locus encoding phosphofructokinase-9 (*PFK9*,
178 PF3D7_0915400) is present in all the suppressed (FSM^S) E2 clones and none of the FSM^R E2
179 clones (Figure 4). *PFK9* is the sole mutated genetic locus that segregates with the change in FSM
180 tolerance.
181
182 *PFK9* encodes phosphofructokinase (PFK, E.C. 2.7.11), which catalyzes the first committed and
183 canonically rate-limiting step of glycolysis, the conversion of fructose 6-phosphate to fructose
184 1,6-bisphosphate. PFK9 is a single polypeptide, comprised of two domains, alpha and beta
185 (Mony, Mehta, Jarori, & Sharma, 2009) (Figure 5A). While in other eukaryotic systems, the
186 alpha domain is typically regulatory, previous work on *P. falciparum* PFK9 has demonstrated
187 catalytic activity for both domains (Bär, Golbik, Hübner, & Kopperschläger, 2000; Kemp &
188 Gunasekera, 2002; Klinder, Kirchberger, Edelmann, & Kopperschläger, 1998; Mony et al., 2009;
189 Theodorou, Cornel, Duff, & Plaxton, 1992).
190
191 We evaluated the effects of the *pfk9*^{T1206I} allele on native PFK activity in *P. falciparum* (Beutler,
192 1984; Mony et al., 2009) (Figure 5B, Figure 5-figure supplement 1). Lysates from both strains
193 possessing the *pfk9*^{T1206I} mutation (E2-S1, S2) have markedly reduced PFK activity compared to
194 the parental strain (*PFK9*).
195

196 **Loss of HAD2 leads to dysregulation of glycolysis at PFK9**

197 Since decreased PFK9 activity restored FSM sensitivity to *had2* mutant strains, we postulated
198 that HAD2 normally regulates glycolysis, perhaps at the step catalyzed by PFK9. To evaluate
199 this possibility, we performed targeted metabolic profiling on the parental parasite strain as well
200 as E2 clones R1-R3 and S1-S2 (Figure 5D). Levels of the MEP pathway intermediate DOXP are
201 significantly increased in FSM^R strains lacking HAD2 (Figure 5D, $p \leq 0.05$, one-way ANOVA).
202 As DOXP is the substrate for the FSM target enzyme DXR, our data indicate that FSM^R strain
203 E2 has become FSM resistant because increased levels of DOXP counteract competitive
204 inhibition of DXR by FSM. We also observe increases in the downstream MEP metabolite,
205 MEcPP, in our FSM^R strains.

206

207 To understand the role of PFK9 in suppressing FSM resistance, we also determined the steady-
208 state levels of glycolytic intermediates (Figure 5D). We find levels of DOXP and MEcPP are
209 tightly correlated with cellular levels of the PFK9 product, FBP (Pearson $r \geq 0.9$, $p \leq 0.01$).
210 Clustering indicates that resistant clones are characterized by a metabolic signature of increased
211 levels of FBP, DOXP, and MEcPP (Figure 5D). Our results suggest that HAD2 controls
212 metabolic homeostasis at the PFK step. Of note, the $pfk9^{T1206I}$ suppressor allele restores nearly
213 parental levels of FBP and downstream MEP pathway intermediates (Figure 5D). Thus, the
214 hypomorphic allele of *PFK9* suppresses the metabolic dysregulation caused by loss of HAD2.

215

216 **Suppression and complementation support model of HAD2- and PFK9-**
217 **mediated metabolic regulation**

218 We propose a model of HAD2/PFK9-mediated metabolic regulation (Figure 6). Our data
219 indicate that HAD2 modulates metabolism through nucleotide dephosphorylation and ultimately
220 restricts glycolysis at the level of PFK9. Loss of HAD2 misroutes metabolism, leading to
221 increased substrate availability to the MEP pathway. This results in a substantial fitness cost in
222 asexual growth, which is rescued by reduced PFK9 activity.
223
224 In further support of this model, we independently repeated our genetic selection with three
225 FSM^R E2 clones (*had2*^{R157X}, *PFK9*^{WT}), cultured without FSM for >1 month (Figure 4). As before,
226 these strains also lost their FSM resistance phenotype (Figure 4) and restored normal growth
227 (Figure 3). We sequenced *HAD2* and *PFK9* in these three suppressed strains (E2-S3, -S4, and -
228 S5). We find that all strains again maintain the *had2*^{R157X} mutation and acquire new, independent
229 *PFK9* mutations, correlating with increased growth rate and FSM sensitivity (Figures 3 and 4).
230 Of the four PFK9 variants identified in this study, three variants map to the alpha domain, while
231 one variant (S335L) maps to the beta domain (Figure 5A). As with the original T1206I variant
232 found in strains S1 and S2, these additional variants show a significant reduction in PFK activity
233 from lysate (Figure 5B).
234
235 Our model also predicted that restoration of functional HAD2 in FSM^R strain E2 should restore
236 FSM sensitivity. Using a piggyback transposon system to express GFP-tagged HAD2 (Balu,
237 Shoue, Fraser, & Adams, 2005; Guggisberg, Park, et al., 2014; Muralidharan, Oksman, Pal,
238 Lindquist, & Goldberg, 2012), we were repeatedly unable to obtain successful transfectants from
239 the FSM^R clones (*had2*^{R157X}, *PFK9*), perhaps due to reduced overall fitness. However, we were
240 able to rescue loss of HAD2 in a suppressed FSM^S E2 clone (*had2*^{R157X}, *pfk9*^{T1206I}) (Figure 5-

241 figure supplement 2A). Consistent with our model, expression of HAD2-GFP in *had2*^{R157X},
242 *pfk9*^{T1206I} parasites led to FSM hyper-sensitivity (Figure 5E, Figure 5-figure supplement 2B).
243 The existence of the *pfk9*^{T1206I} allele in the presence of functional HAD2 seems to reduce parasite
244 fitness, as evidenced by reduced growth (Figure 3, grey vs. teal lines).
245
246
247
248 Using fluorescence microscopy, we observe that HAD2-GFP is localized throughout the
249 cytoplasm in asexual *P. falciparum* trophozoites and schizonts (Figure 5-figure supplement 2C),
250 but excluded from the digestive food vacuole. This is consistent with the lack of a predicted
251 signal sequence for HAD2 using SignalP, PlasmoAP, and PlasMit algorithms (Foth et al., 2003;
252 Petersen, Brunak, von Heijne, & Nielsen, 2011; Zuegge, Ralph, Schmuker, McFadden, &
253 Schneider, 2001). Overall, our localization suggests that HAD2 primarily accesses
254 monophosphorylated nucleotides in the cytosol.
255

256 Discussion

257
258 Cells must control levels of critical metabolites in order to efficiently utilize carbon sources for
259 energy and biosynthesis of essential molecules. Cells may regulate their metabolism via
260 transcriptional, post-transcriptional, post-translational, allosteric, or enzymatic mechanisms that
261 are necessary for growth (Blume et al., 2015; Brown, Brown, Netea, & Gow, 2014; Jurica et al.,
262 1998; Kronstad et al., 2012). In the glucose-rich red blood cell niche, *Plasmodium* spp. malaria
263 parasites display a unique dependence on glycolysis for energy and biosynthesis.

264

265 Using resistance to a metabolic inhibitor, we identify a nucleotidase, HAD2, as a novel regulator
266 of metabolism. Cells lacking HAD2 exhibit marked dysregulation of central carbon metabolism,
267 including altered steady-state levels of glycolytic intermediates and isoprenoid precursors.
268 HAD2 is necessary for optimum parasite fitness, and strains lacking HAD2 acquire additional
269 genetic changes that suppress HAD2-mediated drug resistance and growth defect. We find that
270 mutations in phosphofructokinase (*PFK9*) restore wild-type growth rates and FSM sensitivity.
271 Our study thus directly genetically connect the function of HAD2, a HAD superfamily member,
272 to control of essential central carbon metabolism, as outlined in our model (Figure 6).
273

274 In our study, we find that inhibitor resistance is defined by a distinct metabolic signature,
275 characterized by increased levels of the MEP pathway metabolites DOXP and MEcPP and the
276 key glycolytic metabolite FBP. This finding suggests that MEP pathway metabolism is precisely
277 linked to FBP production. In other microbial systems, FBP levels reflect metabolic flux and are
278 cued to environmental perturbations (Kochanowski et al., 2012). FBP-centered metabolic
279 regulation is also important to the related apicomplexan *Toxoplasma gondii*, which constitutively
280 expresses the fructose 1,6-bisphosphatase (FBPase) to fine-tune glucose metabolism (Blume et
281 al., 2015). While *P. falciparum* does not appear to possess an FBPase, necessary for
282 gluconeogenesis, the parasite may possess alternative FBP-sensing mechanisms to tune
283 metabolism, perhaps via regulators such as HAD1 and HAD2.
284

285 HAD2 is a member of the HAD superfamily and a homolog of the previously described
286 metabolic regulator HAD1. With our previous studies on HAD1 (Guggisberg, Park, et al., 2014;

287 Park, Guggisberg, Odom, & Tolia, 2015), we define the role of these proteins in *P. falciparum*
288 and contribute to the greater understanding of the HADs, an evolutionarily conserved and
289 widespread protein family. Both enzymes belong to the IIB (IPR006379) and Cof-like hydrolase
290 (IPR000150) subfamilies (Hunter et al., 2012). HAD enzymes display diverse substrate
291 preferences (Cabello-Díaz et al., 2015; José A Caparrós-Martín, McCarthy-Suárez, & Culiáñez-
292 Macià, 2013; José Antonio Caparrós-Martín, Reiland, Köchert, Cutanda, & Culiáñez-Macià,
293 2007; Huang et al., 2015; Kuznetsova et al., 2006; Liu et al., 2015; Roberts et al., 2005; Titz et
294 al., 2007), and their biological functions are largely unknown. These subfamilies are comprised
295 of proteins from bacteria and plastid-containing organisms (plants and apicomplexans), most of
296 which notably also employ the MEP pathway, suggesting a common function of HADs. As *P.*
297 *falciparum* HADs influence easily quantified phenotypes (drug tolerance, growth, metabolite
298 levels), the malaria parasite remains an attractive system to study general HAD biology and
299 function.
300
301 Our study uncovers two critical, parasite-specific features of metabolism that are required for *P.*
302 *falciparum* fitness. First, our data indicate that HAD2 is necessary for efficient asexual
303 replication in *P. falciparum*. As HAD2 lacks close mammalian homologs, targeted therapeutics
304 directed against HAD2 are of great interest. Second, our work highlights the central role of the
305 glycolytic enzyme PFK9. While the parasite tolerates substantial reductions in PFK activity in
306 the $had2^{R157X}$ background, such defects reduce the fitness of parasites rescued with HAD2-GFP.
307 A recent kinetic model of parasite glycolysis confirms that PFK has a high flux-control
308 coefficient, is sensitive to competitive inhibition, and can effectively reduce glycolytic flux
309 (Penkler et al., 2015; van Niekerk, Penkler, du Toit, & Snoep, 2016). We thus propose that PFK9

310 is a leading candidate for strategies to target essential glucose metabolism in malaria. Like
311 HAD2, PFK9 is plant-like and evolutionarily divergent from its mammalian homologs (Mony et
312 al., 2009). These differences may be exploited for PFK inhibitor design.
313
314 Finally, our approach demonstrates the power of forward genetics to uncover novel biology in a
315 clinically relevant, non-model organism. We employ a previously described screen for FSM
316 resistance (Guggisberg, Park, et al., 2014) to uncover a novel resistance locus and employ a
317 second selection for parasite fitness to identify changes that suppress our resistance phenotype.
318 While fitness costs associated with antimalarial resistance are well known [summarized in
319 (Gabryszewski et al., 2016; Hastings & Donnelly, 2005; Rosenthal, 2013)], this study represents,
320 to our knowledge, the first to harness this evolutionary trade-off to identify suppressor mutations
321 in a non-target locus. Fitness assessment of resistance mutations may allow for suppressor
322 screening for other antimalarials or other target pathways to reveal new aspects of biology and
323 drug resistance.
324
325

326 # Materials & Methods

327

328 ## Parasite culture maintenance

329 Unless otherwise indicated, parasites were maintained in a 2% suspension of human erythrocytes
330 in RPMI medium (Sigma Aldrich, St. Louis, MO) modified with 27 mM $NaHCO_3$, 11 mM
331 glucose, 5 mM HEPES, 0.01 mM thymidine, 1 mM sodium pyruvate, 0.37 mM hypoxanthine, 10
332 µg/mL gentamycin, and 5 g/L Albumax (Thermo Fisher Scientific, Waltham, MA). Parasites
333 were maintained at 37 °C in 5% O_2/5% CO_2/90% N_2.

334

335 ## Generation of FSM^R strain E2 and clones

336 FSM^R strain E2 was generated as previously described (Guggisberg, Park, et al., 2014). Briefly, a
337 clone of genome reference strain 3D7 (MRA-102, MR4, ATCC, Manassas, VA) was selected
338 with 3 µM FSM. Clones of strain E2 were isolated by limiting dilution.

339

340 ## Quantification of FSM resistance

341 Assays were performed in opaque 96-well plates with FSM concentrations ranging from 0.63 nM
342 to 1 mM. Asynchronous cultures were seeded at 0.5-1.0% parasitemia. After 3 days, media was
343 removed and parasitemia was measured by DNA content using Picogreen fluorescence as
344 previously described (Corbett et al., 2004). Cells were stained for 10 min in a solution containing
345 10 mM Tris HCl, 1 mM EDTA, 2% Triton-X 100, and 0.5% Picogreen reagent (Thermo Fisher
346 Scientific). Fluorescence was measured on a POLARStar Omega spectrophotometer (BMG
347 Labtech, Ortenberg, Germany). Half maximal inhibitory concentration (IC_{50}) values were

348 calculated using Graphpad Prism software (Graphpad Software, La Jolla, CA). At minimum, all
349 assays were performed in triplicate.
350

351 ## Quantitative PCR

352 Total RNA was extracted from saponin-lysed parasites using the Ambion Purelink RNA Mini kit
353 (Thermo Fisher Scientific) according to kit instructions. An on-column DNase (Qiagen, Venlo,
354 Netherlands) treatment was performed after the first wash step. To synthesize cDNA, one
355 microgram of total RNA was used in reverse transcriptase reactions using the Quantitect Reverse
356 Transcription kit (Qiagen).
357
358 PCR reactions were run using Fast SYBR Green PCR Master Mix (Applied Biosystems,
359 Waltham, MA) and 300 nM each primer. Primers used are listed in Supplementary File 1.
360
361 Thermocycling was performed on an Applied Biosystems 7500 Fast RT PCR System with the
362 following parameters: 95 °C for 30 seconds and 40 cycles of 95 °C for 3 seconds, 60 °C for 30
363 seconds. Controls lacking reverse transcriptase and template both produced no significant signal.
364 Melt curve analysis was used to verify that all primer sets produce single products.
365
366 Relative expression levels were calculated using the $\Delta\Delta C_t$ method. ΔC_t represents the C_t value of
367 the reference genes (average of *beta tubulin* and *18s rRNA*) subtracted from the target. $\Delta\Delta C_t$
368 represents the ΔC_t value of the parental sample subtracted from the sample of interest. Fold
369 changes are calculated as $2^{-\Delta\Delta Ct}$. All assays were performed using technical and biological
370 triplicates.

371

372

373 **Antisera generation**

374 Anti-HAD1 antisera has been previously described (MRA-1256, MR4, ATCC, Manassas, VA)
375 (Guggisberg, Park, et al., 2014). Polyclonal anti-HAD2 antisera was raised against 6xHis-HAD2
376 in rabbits, with Titermax as an adjuvant (Cocalico Biologicals, Reamstown, PA). Antisera
377 specificity was confirmed by immunoblot of *P. falciparum* lysate lacking HAD2.

378

379 **Immunoblotting**

380 Lysates were separated on a polyacrylamide gel and transferred to a polyvinylidene difluoride
381 membrane. Membranes were blocked in 5% non-fat dry milk, 0.1% Tween-20 in PBS. Rabbit
382 polyclonal antisera were used at the following dilutions: anti-HAD2, 1:2,000-5,000; anti-HAD1
383 (Guggisberg, Park, et al., 2014), 1:20,000; anti-heat shock protein 70 (Hsp70), 1:5,000 (AS08
384 371, Agrisera Antibodies, Vännäs, Sweden). All blots used an HRP-conjugated goat anti-rabbit
385 IgG secondary antibody at 1:20,000 (ThermoFisher Scientific 65-6120). When necessary, blots
386 were stripped by washing with 200 mM glycine, 0.1% SDS, 1% Tween-20, pH 2.2 before re-
387 probing.

388

389 **Whole genome sequencing and SNP analysis**

390 Library preparation, Illumina sequencing, read alignment, and variant analysis were performed
391 by the Washington University Genome Technology Access Center (GTAC, St. Louis, MO).
392 Parasite genomic DNA was prepared for sequencing as previously described (Guggisberg, Park,
393 et al., 2014). One microgram of genomic DNA was sheared, end repaired, and adapter ligated.

394 Libraries were sequenced on an Illumina HiSeq 2500 in Rapid Run mode to generate 101 bp
395 paired end reads. Reads were aligned to the *P. falciparum* 3D7 reference genome (PlasmoDB
396 v7.2) using Novoalign (V2.08.02). Duplicate reads were removed. SNPs were called using
397 samtools, using a quality score cutoff of 20 and a read depth cutoff of 5. SNPs were annotated
398 using snpEff. Parental SNPs were removed using previously sequenced parental genomes
399 (Guggisberg, Park, et al., 2014). Data has been deposited in the NCBI BioProject database
400 (PRJNA222697) and Sequence Read Archive (SRP038937).
401

402 **Sanger sequencing**

403 The E2 A469T (R157X) *HAD2* SNP was verified by amplifying *P. falciparum* genomic DNA
404 using primers HAD2_R157X_F and HAD2_R157X_R. The *PFK9* locus was amplified using the
405 PFK9_F and PFK9_R primers. Amplicons were sequenced using the PFK9_seq_(1-8) primers.
406 Primer sequences can be found in Supplementary File 1.
407

408 **Generation of recombinant protein**

409 The predicted coding sequence of *HAD2* (PlasmoDB ID PF3D7_1226300) was amplified from *P.*
410 *falciparum* genomic DNA by PCR using the HAD2_LIC_F and HAD2_LIC_R primers
411 (Supplementary File 1). Ligation-independent cloning was used to clone the PCR product into
412 vector BG1861 (Alexandrov et al., 2004), which introduces an N-terminal 6xHis fusion to the
413 expressed protein. BG1861:6xHis-HAD2 construct was transformed into One Shot
414 BL21(DE3)pLysS *Escherichia coli* cells (Thermo Fisher Scientific) according to supplier
415 instructions. Protein expression was induced for 3 hours with isopropyl-β-D-thiogalactoside at
416 mid-log phase (OD_{600} 0.4 – 0.5). Cells were collected by centrifugation and stored at -20°C.

417

418 Induced cell pellets were lysed in buffer containing 1 mg/mL lysozyme, 20 mM imidazole, 1 mM
419 dithiothreitol, 10 mM Tris HCl (pH 7.5), 30 U benzonase (EMD Millipore, Darmstadt, Germany),
420 and Complete Mini EDTA-free protease inhibitor tablets (Roche Applied Science, Penzberg,
421 Germany). 6xHis-HAD2 was bound to nickel agarose beads (Gold Biotechnology, Olivette, MO)
422 and eluted in 300 mM imidazole, 20mM Tris HCl (pH 7.5), and 150 mM NaCl. This eluate was
423 further purified by size-exclusion gel chromatography using a HiLoad 16/600 Superdex 200 pg
424 column (GE Healthcare, Chicago, IL) equilibrated in 50 mM Tris HCl (pH 7.5), 1 mM
425 dithiothreitol, and 1 mM $MgCl_2$. The elution fractions containing HAD2 were pooled into a
426 centrifugal filter and concentrated to approximately 3 mg/ml. Glycerol was added to a final
427 concentration of 10% (w/v), and the solution was immediately flash frozen in liquid nitrogen and
428 stored at -80°C. The purification of recombinant HAD1 has been previously described
429 (Guggisberg, Park, et al., 2014).

430

431 **HAD2 activity assays**

432 Recombinant 6xHis-HAD2 was generated in *E. coli*. HAD2 phosphatase activity was measured
433 against the substrate *p*NPP (New England Biolabs, Ipswich, MA). Phosphatase activity of
434 recombinant enzyme was initially evaluated against the substrate *para*-nitrophenyl phosphate
435 (New England Biolabs). Reactions contained 10 mM *p*NPP, 50 mM Tris HCl (pH 7.5), 5 mM
436 $MgCl_2$, 0.5 mM $MnCl_2$, and 0.25-4 μg enzyme. *Para*-nitrophenyl production was quantified by
437 absorbance at 405 nm. All reactions were performed at 37°C.

438

439 Specific enzyme activity against phosphorylated substrates was measured using the EnzChek
440 Phosphate Assay Kit (Thermo Fisher Scientific) according to supplier instructions. Reactions
441 were performed in 50 µL volumes containing 1 mM substrate and 150–750 ng enzyme. Kinetic
442 parameters were determined by continuous measurement of product formation in response to
443 0.06 – 10 mM substrate. All reactions were performed at 37°C.
444

445 **Metabolic profiling**

446 All metabolic profiling was performed on ~1 x 10^9 early trophozoites synchronized by treatment
447 with 5% sorbitol. Parasite-infected erythrocytes were lysed with saponin, washed with cold 2 g/L
448 glucose in PBS, and frozen at -80 °C. For measurement of nucleotide levels, samples were
449 extracted and prepared for ultra-high performance liquid chromatography tandem mass
450 spectrometry (IP-RP–UPLC–MS/MS) as previously described (Laourdakis et al., 2014).
451

452 For measurement of MEP pathway and glycolytic intermediates, samples were extracted in 600
453 µL of ice-cold extraction solvent [chloroform, methanol, and acetonitrile (2:1:1, v/v/v)] using
454 two liquid-nitrogen cooled 3.2 mm stainless steel beads and homogenization in a Tissue-Lyser II
455 instrument (Qiagen) at 20 Hz for 5 minutes in a cold sample rack. Ice-cold water was added and
456 samples were homogenized for 5 more minutes at 20 Hz. Samples were centrifuged at 14,000 rcf
457 at 4°C for 5 min. The polar phase was lyophilized and re-dissolved in 100 µL water and analyzed
458 by LC-MS/MS. LC-MS/MS was performed on a 4000QTRAP system (AB Sciex, Framingham,
459 MA) in multiple-reaction monitoring mode using negative ioniziation and 10 mM
460 tributylammonium acetate (pH 5.1-5.5) as the ion pair reagent. The specific parameters used for
461 analysis of MEP pathway metabolites have been previously described (Zhang et al., 2011).

462 Liquid chromatography separation was performed using ion pair reverse-phase chromatography
463 (Luo, Groenke, Takors, Wandrey, & Oldiges, 2007). The referenced method (Luo et al., 2007)
464 was modified: (1) RP-hydro 100 mm × 2.0 mm, 2.5 µm high performance liquid chromatography
465 column (Phenomenex, Torrance, CA), (2) flow rate of 0.14 mL/min, (3) solvent A of 10 mM
466 tributylammonium acetate in 5% methanol, (4) binary LC gradient (20% solvent B (100%
467 methanol) from 0 to 2.5 min, 30% B for 12.5 min, 80% B for 5 min, and column equilibration at
468 for 5 minutes), and (5) 20 µL autosampler injection volume.
469

470 ## *P. falciparum* growth assays

471 Asynchronous cultures were seeded at 1% parasitemia (percent of infected red blood cells).
472 Media was exchanged daily. All assays were performed in the absence of drug pressure. Samples
473 were fixed in 4% paraformaldehyde, 0.05% glutaraldehyde in PBS. Fixed samples were stained
474 with 0.01 mg/ml acridine orange and parasitemia was determined on a BD Biosciences LSRII
475 flow cytometer (Thermo Fisher Scientific). All assays were performed using biological
476 triplicates, at minimum.
477

478 ## Assay of PFK9 activity from lysate

479 Sorbitol-synchronized trophozites were isolated using 0.1% saponin. Cell pellets were washed
480 three times in buffer [100 mM Tris-HCl (pH 7.5), 1 mM $MgCl_2$, 1 mM DTT, 10% glycerol, and
481 EDTA-free protease inhibitor tablets (Roche)]. Lysates were prepared by sonication at 4°C
482 (Fisher Scientific Model 550 Sonic Dismembrator, amplitude 3.5), followed by centrifugation at
483 4°C (10,000 x *g*, 10 min).
484

485 PFK9 activity in lysate was monitored by linking it to the oxidation of NADH, as described
486 previously (Beutler, 1984; Mony et al., 2009). Reactions contained 100 mM Tris-HCl (pH 7.5), 1
487 mM $MgCl_2$, 1 mM DTT, 0.25 mM NADH, 1 mM ATP, 3 mM fructose 6-phosphate, as well as
488 excess of linking enzymes aldolase (7.5 U), triose-phosphate isomerase (3.8 U), and glycerol 3-
489 phosphate dehydrogenase (3.8 U). After adding fresh cell lysate (15 µg total protein), the
490 absorbance at 340 nm was measured at 37°C for 40 min. Activity (µmol/min/mg total protein)
491 was determined by linear regression using Graphpad Prism software. All assays were performed
492 using technical and biological triplicates.
493

494 **pTEOE110:HAD2 plasmid construction**

495 The pTEOE110:HAD2-GFP construct contains the *heat shock protein 110* (PF3D7_0708800) 5'
496 UTR and a C-terminal GFP tag. Human dihydrofolate reductase (hDHFR) is present as a
497 selectable marker. Inverted terminal repeats are included for integration into the genome by a co-
498 transfected piggyBac transposase (pHTH, MRA912, MR4, ATCC, Manassas, VA).
499

500 *HAD2* was amplified with the HAD2_XhoI_F and HAD2_AvrII_R primers (Supplementary File
501 1) and cloned into AvrII and XhoI sites in the pTEOE110 plasmid.
502

503 **Parasite transfections**

504 Transfections were performed as previously described (Guggisberg, Park, et al., 2014). Briefly,
505 50-100 µg of plasmid DNA was precipitated and resuspended in Cytomix (25 mM HEPES pH
506 7.6, 120 mM KCl, 0.15 mM $CaCl_2$, 2mM EGTA, 5 mM $MgCl_2$, 10 mM K_2HPO_4).
507

508 A ring-stage *P. falciparum* culture was washed with Cytomix and resuspended in the
509 DNA/Cytomix solution. The culture was electroporated at 950 µF and 0.31 kV, washed with
510 media, and returned to normal culture conditions. Parasites expressing the construct were
511 selected by continuous treatment with 5 nM WR92210 (Jacobus Pharmaceuticals, Princeton, NJ).
512 Transfectants were cloned by limiting dilution and presence of the HAD2-GFP construct was
513 verified by PCR using gene-specific and GFP-specific primers (HAD2_R157X_F and GFP_R,
514 Supplementary File 1). The presence of the endogenous $had2^{R157X}$ and $pfk9^{T1206I}$ mutations were
515 verified by Sanger sequencing.
516

517 **Live fluorescent microscopy**

518 Erythrocytes infected with E2 Hsp110:HAD2-GFP parasites were stained with 10 ng/µL Hoescht
519 33258 and mounted under coverslips on polysine adhesion slides. Cells were viewed on an
520 Olympus BH8 microscope (Tokyo, Japan). Minimal adjustments to contrast and brightness were
521 applied equally to all microscopy images using Inkscape.
522

523 ## Author contributions

524 Conceptualization, A.M.G., A.Y.G., and A.R.O.J.; Investigation, A.M.G., A.Y.G., E.F.M., and
525 M.B.C.; Resources, A.M.G. and S.J.E.; Writing – Original Draft, A.M.G. and A.R.O.J.; Writing
526 – Review and Editing, A.M.G., A.Y.G., S.J.E., E.F.M, M.B.C, and A.R.O.J; Visualization,
527 A.M.G. and A.Y.G.; Supervision, A.R.O.J.; Funding acquisition, A.R.O.J.
528

529 ## Acknowledgments

530 This work is supported by the NIH/NIAID (R01AI103280 to A.R.O.J. and AI108819 to M.B.C.),
531 the Children's Discovery Institute of Washington University and St. Louis Children's Hospital
532 (MD-LI-2011-171 to A.R.O.J.), the March of Dimes Foundation (Basil O'Connor Starter Scholar
533 Research Award to A.R.O.J.), the Doris Duke Foundation (Clinical Scientist Development
534 Award to A.R.O.J.), the NIH/NIGMS (training grant T32GM007067 to A.M.G.), the Monsanto
535 Excellence Fund at Washington University (graduate fellowship to A.M.G.), a HHMI Summer
536 Undergraduate Research Fellowship (to A.Y.G.), and an ASM Undergraduate Research
537 Fellowship (to A.Y.G.). We thank the Proteomics and Mass Spectrometry Facility at the Donald
538 Danforth Plant Science Center for assistance with LC-MS/MS. This work was supported by the
539 National Science Foundation under grant number DBI-0521250 for acquisition of the QTRAP
540 LC-MS/MS. We thank Daniel Goldberg (Washington University) for supplying the pTEOE110
541 plasmid. We thank the Malaria Research Reference and Reagent Resource (MR4) for providing
542 reagents contributed by D.J. Carucci (MRA-102) and John Adams (MRA-912).
543

References

Alexandrov, A., Vignali, M., LaCount, D. J., Quartley, E., de Vries, C., De Rosa, D., … Grayhack, E. J. (2004). A facile method for high-throughput co-expression of protein pairs. *Molecular & Cellular Proteomics*, *3*(9), 934–8.

Aurrecoechea, C., Brestelli, J., Brunk, B. P., Dommer, J., Fischer, S., Gajria, B., … Wang, H. (2009). PlasmoDB: a functional genomic database for malaria parasites. *Nucleic Acids Research*, *37*(Database issue), D539-43.

Balu, B., Shoue, D. A., Fraser, M. J., & Adams, J. H. (2005). High-efficiency transformation of *Plasmodium falciparum* by the lepidopteran transposable element piggyBac. *Proceedings of the National Academy of Sciences of the United States of America*, *102*(45), 16391–6.

Bär, J., Golbik, R., Hübner, G., & Kopperschläger, G. (2000). Denaturation of phosphofructokinase-1 from *Saccharomyces cerevisiae* by guanidinium chloride and reconstitution of the unfolded subunits to their catalytically active form. *Biochemistry*, *39*(23), 6960–8.

Beutler, E. (1984). *Red Cell Metabolism: A Manual of Biochemical Methods*. Philadelphia, PA: Grune & Stratton.

Blume, M., Nitzsche, R., Sternberg, U., Gerlic, M., Masters, S. L., Gupta, N., & McConville, M. J. (2015). A *Toxoplasma gondii* gluconeogenic enzyme contributes to robust central carbon metabolism and is essential for replication and virulence. *Cell Host & Microbe*, *18*(2), 210–20.

Bowman, I. B., Grant, P. T., Kermack, W. O., & Ogston, D. (1961). The metabolism of *Plasmodium berghei*, the malaria parasite of rodents. 2. An effect of mepacrine on the metabolism of glucose by the parasite separated from its host cell. *The Biochemical Journal*, *78*(3), 472–8.

Brown, A. J. P., Brown, G. D., Netea, M. G., & Gow, N. A. R. (2014). Metabolism impacts upon Candida immunogenicity and pathogenicity at multiple levels. *Trends in Microbiology*, *22*(11), 614–622.

Burroughs, A. M., Allen, K. N., Dunaway-Mariano, D., & Aravind, L. (2006). Evolutionary genomics of the HAD superfamily: understanding the structural adaptations and catalytic diversity in a superfamily of phosphoesterases and allied enzymes. *Journal of Molecular Biology*, *361*(5), 1003–34.

Cabello-Díaz, J. M., Gálvez-Valdivieso, G., Caballo, C., Lambert, R., Quiles, F. A., Pineda, M., & Piedras, P. (2015). Identification and characterization of a gene encoding for a nucleotidase from *Phaseolus vulgaris*. *Journal of Plant Physiology*, *185*, 44–51.

Caparrós-Martín, J. A., McCarthy-Suárez, I., & Culiáñez-Macià, F. A. (2013). HAD hydrolase function unveiled by substrate screening: enzymatic characterization of *Arabidopsis thaliana* subclass I phosphosugar phosphatase AtSgpp. *Planta*, *237*(4), 943–54.

Caparrós-Martín, J. A., Reiland, S., Köchert, K., Cutanda, M. C., & Culiáñez-Macià, F. A. (2007). *Arabidopsis thaliana* AtGppl and AtGpp2: two novel low molecular weight phosphatases involved in plant glycerol metabolism. *Plant Molecular Biology*, *63*(4), 505–17.

Corbett, Y., Herrera, L., Gonzalez, J., Cubilla, L., Capson, T. L., Coley, P. D., … Ortega-Barria, E. (2004). A novel DNA-based microfluorimetric method to evaluate antimalarial drug activity. *American Journal of Tropical Medicine and Hygiene*, *70*(2), 119–24.

Emami, S. N., Lindberg, B. G., Hua, S., Hill, S., Mozuraitis, R., Lehmann, P., … Faye, I. (2017).

590 A key malaria metabolite modulates vector blood seeking, feeding, and susceptibility to
591 infection. *Science*, *355*(6329), 1076–1080.
592 Foth, B. J., Ralph, S. A., Tonkin, C. J., Struck, N. S., Fraunholz, M., Roos, D. S., … McFadden,
593 G. I. (2003). Dissecting apicoplast targeting in the malaria parasite *Plasmodium falciparum*.
594 *Science*, *299*(5607), 705–8.
595 Gabryszewski, S. J., Dhingra, S. K., Combrinck, J. M., Lewis, I. A., Callaghan, P. S., Hassett, M.
596 R., … Fidock, D. A. (2016). Evolution of fitness cost-neutral mutant PfCRT conferring *P.*
597 *falciparum* 4-aminoquinoline drug resistance is accompanied by altered parasite metabolism
598 and digestive vacuole physiology. *PLOS Pathogens*, *12*(11), e1005976.
599 Gershenzon, J., & Dudareva, N. (2007). The function of terpene natural products in the natural
600 world. *Nature Chemical Biology*, *3*(7), 408–14.
601 Gisselberg, J. E., Dellibovi-Ragheb, T. A., Matthews, K. A., Bosch, G., & Prigge, S. T. (2013).
602 The Suf iron-sulfur cluster synthesis pathway is required for apicoplast maintenance in
603 malaria parasites. *PLoS Pathogens*, *9*(9), e1003655.
604 Guggisberg, A. M., Amthor, R. E., & Odom, A. R. (2014). Isoprenoid biosynthesis in
605 Plasmodium falciparum. *Eukaryotic Cell*, *13*(11), 1348–59.
606 Guggisberg, A. M., Kelly, M. L., Hodge, D. M., & Odom, A. R. (2013a). Fosmidomycin-
607 resistant *Plasmodium falciparum* whole genome sequencing. *NCBI BioProject Database*,
608 (PRJNA222697).
609 Guggisberg, A. M., Kelly, M. L., Hodge, D. M., & Odom, A. R. (2013b). Fosmidomycin-
610 resistant *Plasmodium falciparum* whole genome sequencing. *Sequence Read Archive*,
611 (SRP038937).
612 Guggisberg, A. M., Park, J., Edwards, R. L., Kelly, M. L., Hodge, D. M., Tolia, N. H., & Odom,
613 A. R. (2014). A sugar phosphatase regulates the methylerythritol phosphate (MEP) pathway
614 in malaria parasites. *Nature Communications*, *5*, 4467.
615 Hastings, I. M., & Donnelly, M. J. (2005). The impact of antimalarial drug resistance mutations
616 on parasite fitness, and its implications for the evolution of resistance. *Drug Resistance*
617 *Updates*, *8*(1), 43–50.
618 Huang, H., Pandya, C., Liu, C., Al-Obaidi, N. F., Wang, M., Zheng, L., … Farelli, J. D. (2015).
619 Panoramic view of a superfamily of phosphatases through substrate profiling. *Proceedings*
620 *of the National Academy of Sciences of the United States of America*, *112*(16), E1974-83.
621 Retrieved from http://www.ncbi.nlm.nih.gov/pubmed/25848029
622 Hunter, S., Jones, P., Mitchell, A., Apweiler, R., Attwood, T. K., Bateman, A., … Yong, S.-Y.
623 (2012). InterPro in 2011: new developments in the family and domain prediction database.
624 *Nucleic Acids Research*, *40*(Database issue), D306-12.
625 Imlay, L., & Odom, A. R. (2014). Isoprenoid metabolism in apicomplexan parasites. *Current*
626 *Clinical Microbiology Reports*, *1*(3–4), 37–50. http://doi.org/10.1007/s40588-014-0006-7
627 Jordão, F. M., Kimura, E. A., & Katzin, A. M. (2011). Isoprenoid biosynthesis in the
628 erythrocytic stages of Plasmodium falciparum. *Memórias Do Instituto Oswaldo Cruz*, *106*,
629 134–141.
630 Jurica, M. S., Mesecar, A., Heath, P. J., Shi, W., Nowak, T., & Stoddard, B. L. (1998). The
631 allosteric regulation of pyruvate kinase by fructose-1,6-bisphosphate. *Structure*, *6*(2), 195–
632 210.
633 Kang, M. J., Lee, Y. M., Yoon, S. H., Kim, J. H., Ock, S. W., Jung, K. H., … Kim, S. W. (2005).
634 Identification of genes affecting lycopene accumulation in *Escherichia coli* using a shot-gun
635 method. *Biotechnology and Bioengineering*, *91*(5), 636–42.

636 Kang, Y., Weber, K. D., Qiu, Y., Kiley, P. J., & Blattner, F. R. (2005). Genome-wide expression
637 analysis indicates that FNR of *Escherichia coli* K-12 regulates a large number of genes of
638 unknown function. *Journal of Bacteriology*, *187*(3), 1135–1160.
639 Kemp, R. G., & Gunasekera, D. (2002). Evolution of the allosteric ligand sites of mammalian
640 phosphofructo-1-kinase. *Biochemistry*, *41*(30), 9426–30.
641 Klinder, A., Kirchberger, J., Edelmann, A., & Kopperschläger, G. (1998). Assembly of
642 phosphofructokinase-1 from *Saccharomyces cerevisiae* in extracts of single-deletion
643 mutants. *Yeast*, *14*(4), 323–34.
644 Kochanowski, K., Volkmer, B., Gerosa, L., Haverkorn van Rijsewijk, B. R., Schmidt, A., &
645 Heinemann, M. (2012). Functioning of a metabolic flux sensor in *Escherichia coli*.
646 *Proceedings of the National Academy of Sciences*, *110*(3), 1130–1135.
647 Koppisch, A. T., Fox, D. T., Blagg, B. S. J., & Poulter, C. D. (2002). *E. coli* MEP synthase:
648 steady-state kinetic analysis and substrate binding. *Biochemistry*, *41*(1), 236–43.
649 Kronstad, J., Saikia, S., Nielson, E. D., Kretschmer, M., Jung, W., Hu, G., … Attarian, R. (2012).
650 Adaptation of *Cryptococcus neoformans* to mammalian hosts: integrated regulation of
651 metabolism and virulence. *Eukaryotic Cell*, *11*(2), 109–18.
652 Krungkrai, J., Burat, D., Kudan, S., Krungkrai, S., & Prapunwattana, P. (1999). Mitochondrial
653 oxygen consumption in asexual and sexual blood stages of the human malarial parasite,
654 *Plasmodium falciparum*. *The Southeast Asian Journal of Tropical Medicine and Public*
655 *Health*, *30*(4), 636–42.
656 Kuznetsova, E., Proudfoot, M., Gonzalez, C. F., Brown, G., Omelchenko, M. V, Borozan, I., …
657 Yakunin, A. F. (2006). Genome-wide analysis of substrate specificities of the *Escherichia*
658 *coli* haloacid dehalogenase-like phosphatase family. *The Journal of Biological Chemistry*,
659 *281*(47), 36149–61.
660 Kuznetsova, E., Proudfoot, M., Sanders, S. A., Reinking, J., Savchenko, A., Arrowsmith, C. H.,
661 … Yakunin, A. F. (2005). Enzyme genomics: Application of general enzymatic screens to
662 discover new enzymes. *FEMS Microbiology Reviews*, *29*(2), 263–79.
663 Kuzuyama, T., Shimizu, T., Takahashi, S., & Seto, H. (1998). Fosmidomycin, a specific inhibitor
664 of 1-deoxy-d-xylulose 5-phosphate reductoisomerase in the nonmevalonate pathway for
665 terpenoid biosynthesis. *Tetrahedron Letters*, *39*(43), 7913–6.
666 Lange, B. M., Rujan, T., Martin, W., & Croteau, R. (2000). Isoprenoid biosynthesis: the
667 evolution of two ancient and distinct pathways across genomes. *Proceedings of the National*
668 *Academy of Sciences of the United States of America*, *97*(24), 13172–7.
669 Laourdakis, C. D., Merino, E. F., Neilson, A. P., & Cassera, M. B. (2014). Comprehensive
670 quantitative analysis of purines and pyrimidines in the human malaria parasite using ion-
671 pairing ultra-performance liquid chromatography-mass spectrometry. *Journal of*
672 *Chromatography. B, Analytical Technologies in the Biomedical and Life Sciences*, *967*,
673 127–33.
674 Liu, J., Zhou, W., Liu, G., Yang, C., Sun, Y., Wu, W., … Cheng, Y. (2015). The conserved
675 endoribonuclease YbeY is required for chloroplast ribosomal RNA processing in
676 Arabidopsis. *Plant Physiology*, *168*(1), 205–221.
677 Luo, B., Groenke, K., Takors, R., Wandrey, C., & Oldiges, M. (2007). Simultaneous
678 determination of multiple intracellular metabolites in glycolysis, pentose phosphate pathway
679 and tricarboxylic acid cycle by liquid chromatography-mass spectrometry. *Journal of*
680 *Chromatography*, *1147*(2), 153–64.
681 MacRae, J. I., Dixon, M. W., Dearnley, M. K., Chua, H. H., Chambers, J. M., Kenny, S., …

682 McConville, M. J. (2013). Mitochondrial metabolism of sexual and asexual blood stages of
683 the malaria parasite *Plasmodium falciparum*. *BMC Biology*, *11*(1), 67.
684 Mehta, M., Sonawat, H. M., & Sharma, S. (2006). Glycolysis in *Plasmodium falciparum* results
685 in modulation of host enzyme activities. *Journal of Vector Borne Diseases*, *43*(3), 95–103.
686 Mony, B. M., Mehta, M., Jarori, G. K., & Sharma, S. (2009). Plant-like phosphofructokinase
687 from *Plasmodium falciparum* belongs to a novel class of ATP-dependent enzymes.
688 *International Journal for Parasitology*, *39*(13), 1441–53.
689 Muralidharan, V., Oksman, A., Pal, P., Lindquist, S., & Goldberg, D. E. (2012). *Plasmodium*
690 *falciparum* heat shock protein 110 stabilizes the asparagine repeat-rich parasite proteome
691 during malarial fevers. *Nature Communications*, *3*, 1310.
692 Park, J., Guggisberg, A. M., Odom, A. R., & Tolia, N. H. (2015). Cap-domain closure enables
693 diverse substrate recognition by the C2-type haloacid dehalogenase-like sugar phosphatase
694 *Plasmodium falciparum* HAD1. *Acta Crystallographica. Section D, Biological*
695 *Crystallography*, *71*(Pt 9), 1824–34.
696 Penkler, G., du Toit, F., Adams, W., Rautenbach, M., Palm, D. C., van Niekerk, D. D., & Snoep,
697 J. L. (2015). Construction and validation of a detailed kinetic model of glycolysis in
698 *Plasmodium falciparum*. *The FEBS Journal*.
699 Petersen, T. N., Brunak, S., von Heijne, G., & Nielsen, H. (2011). SignalP 4.0: discriminating
700 signal peptides from transmembrane regions. *Nature Methods*, *8*(10), 785–6.
701 Pratish, G., & Radhakrishnan, M. (2014). Engineering *Escherichia coli* for D-ribose production
702 from glucose-xylose mixtures. *Industrial Biotechnology*, *10*(2), 106–114.
703 Roberts, A., Lee, S.-Y., McCullagh, E., Silversmith, R. E., & Wemmer, D. E. (2005). YbiV from
704 *Escherichia coli* K12 is a HAD phosphatase. *Proteins*, *58*(4), 790–801.
705 Rosenthal, P. J. (2013). The interplay between drug resistance and fitness in malaria parasites.
706 *Molecular Microbiology*, *89*(6), 1025–1038.
707 Roth, E. (1990). *Plasmodium falciparum* carbohydrate metabolism: a connection between host
708 cell and parasite. *Blood Cells*, *16*(2–3), 453–66.
709 Roth, E. F. (1987). Malarial parasite hexokinase and hexokinase-dependent glutathione reduction
710 in the *Plasmodium falciparum*-infected human erythrocyte. *The Journal of Biological*
711 *Chemistry*, *262*(32), 15678–82.
712 Scheibel, L. W., & Miller, J. (1969). Glycolytic and cytochrome oxidase activity in Plasmodia.
713 *Military Medicine*, *134*(10), 1074–80.
714 Srinivasan, B., Kempaiah Nagappa, L., Shukla, A., & Balaram, H. (2015). Prediction of substrate
715 specificity and preliminary kinetic characterization of the hypothetical protein PVX_123945
716 from *Plasmodium vivax*. *Experimental Parasitology*, *151*, 56–63.
717 Steinbacher, S., Kaiser, J., Eisenreich, W., Huber, R., Bacher, A., & Rohdich, F. (2003).
718 Structural basis of fosmidomycin action revealed by the complex with 2-C-methyl-D-
719 erythritol 4-phosphate synthase (IspC). Implications for the catalytic mechanism and anti-
720 malaria drug development. *The Journal of Biological Chemistry*, *278*(20), 18401–7.
721 Sun, Y., & Vanderpool, C. K. (2013). Physiological consequences of multiple-target regulation
722 by the small RNA SgrS in *Escherichia coli*. *Journal of Bacteriology*, *195*(21), 4804–15.
723 Theodorou, M. E., Cornel, F. A., Duff, S. M., & Plaxton, W. C. (1992). Phosphate starvation-
724 inducible synthesis of the alpha-subunit of the pyrophosphate-dependent
725 phosphofructokinase in black mustard suspension cells. *The Journal of Biological*
726 *Chemistry*, *267*(30), 21901–5.
727 Titz, B., Häuser, R., Engelbrecher, A., Uetz, P., Alatossava, T., Jutte, H., … Inouye, M. (2007).

The *Escherichia coli* protein YjjG is a house-cleaning nucleotidase in vivo. *FEMS Microbiology Letters*, *270*(1), 49–57.

van Niekerk, D. D., Penkler, G. P., du Toit, F., & Snoep, J. L. (2016). Targeting glycolysis in the malaria parasite *Plasmodium falciparum*. *The FEBS Journal*, *283*(4), 634–46.

Yeh, E., & DeRisi, J. L. (2011). Chemical rescue of malaria parasites lacking an apicoplast defines organelle function in blood-stage *Plasmodium falciparum*. *PLoS Biology*, *9*(8), e1001138.

Zhang, B., Watts, K. M., Hodge, D., Kemp, L. M., Hunstad, D. A., Hicks, L. M., & Odom, A. R. (2011). A second target of the antimalarial and antibacterial agent fosmidomycin revealed by cellular metabolic profiling. *Biochemistry*, *50*(17), 3570–7.

Zuegge, J., Ralph, S., Schmuker, M., McFadden, G. I., & Schneider, G. (2001). Deciphering apicoplast targeting signals--feature extraction from nuclear-encoded precursors of *Plasmodium falciparum* apicoplast proteins. *Gene*, *280*(1–2), 19–26.

743 # Figures and Tables

744

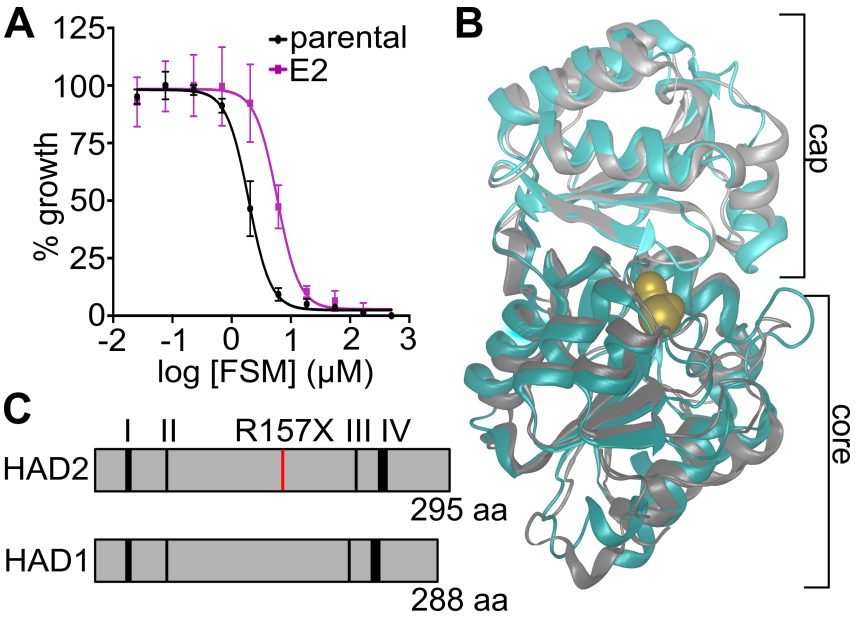

745

746 **Figure 1. FSM^R strain E2 possesses a mutation in HAD2, a homolog of the MEP pathway**

747 **regulator HAD1. (A)** Representative FSM dose-response of the parental strain and strain E2.

748 Strain E2 has a mean IC_{50} of 4.8 ± 1.2 μM (n=7), greater than the parent strain (0.8 ± 0.1 μM),

749 $p \leq 0.01$, unpaired Student's t-test. (**B**) *P. vivax* HAD2 (teal, PDB 2B30) is structurally similar to

750 PfHAD1 (grey, PDB 4QJB). Ions (Mg^{2+}, Ca^{2+}, Cl^-) are shown in yellow. (**C**) HAD2 is a homolog

751 of HAD1 (~29% identity and ~53% similarity) and possesses all HAD conserved sequence

752 motifs required for catalysis (Burroughs, Allen, Dunaway-Mariano, & Aravind, 2006).

753

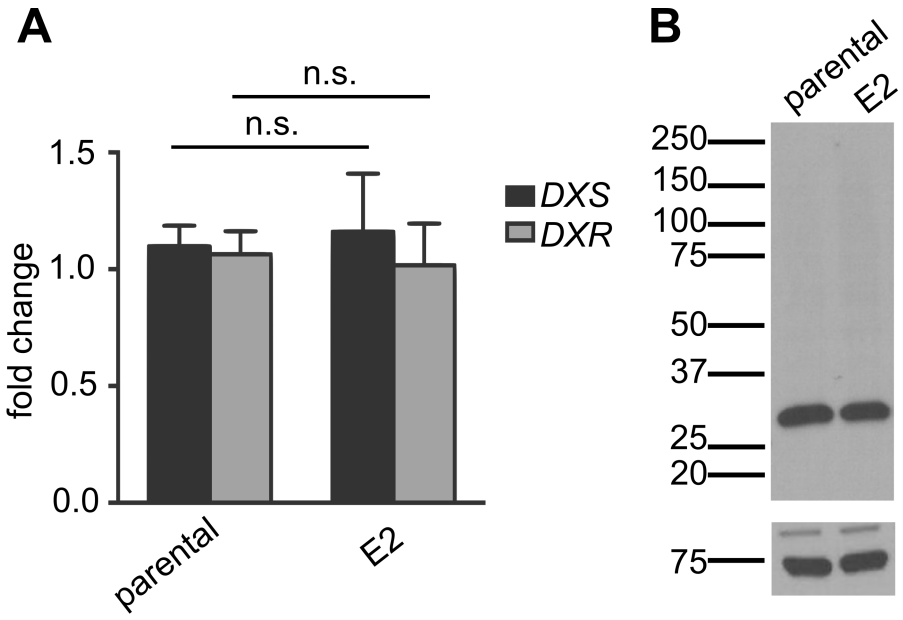

754

755 **Figure 1-figure supplement 1. FSM^R strain E2 does not have increased expression of *DXS*,**

756 ***DXR*, or HAD1.**

757 (**A**) *DXS* and *DXR* transcript levels are unchanged in FSM^R strain E2. Shown are mean relative

758 mRNA expression levels determined by qPCR. Error bars represent S.E.M. from duplicate

759 biological replicates, measured using three technical replicates (N.s. = not significant, p>0.05,

760 unpaired Student's t-test). (**B**) HAD1 expression is unchanged in FSM^R strain E2. Shown are

761 immunoblots of the parent strain and FSM^R strain E2. Marker units are kilodaltons (kDa). Top

762 panel was probed with anti-HAD1 antisera. Bottom panel was probed with anti-heat shock

763 protein 70 antisera as a loading control. Expected protein masses: HAD1, 33 kDa; Hsp70, 74

764 kDa. Blot is representative of three independent experiments. Minimal brightness adjustments

765 were applied equally to all blot images.

766

767

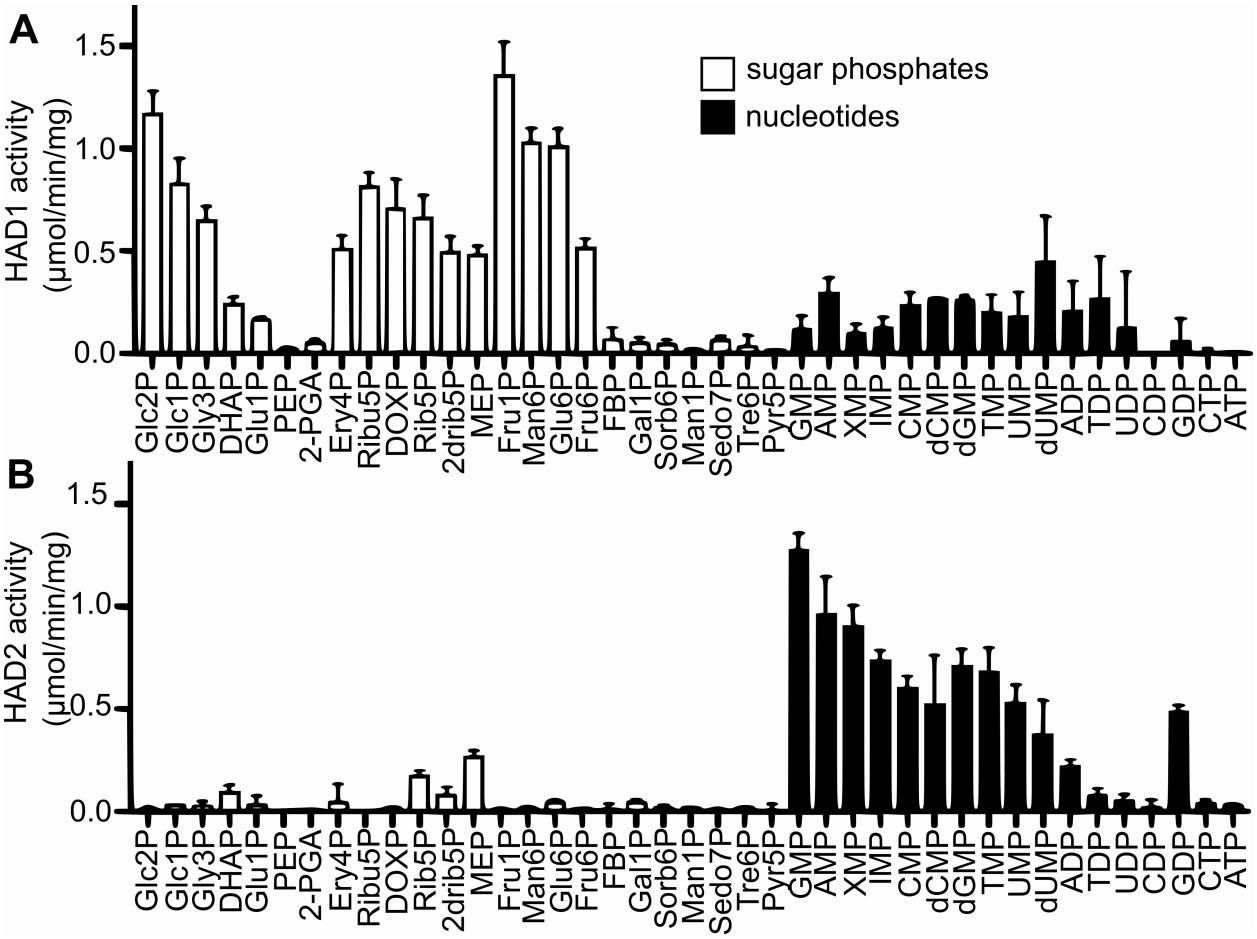

768

769 **Figure 2. HAD2 is a nucleotidase.**

770 Shown are mean specific enzyme activities for (**A**) HAD1 and (**B**) HAD2. Error bars represent
771 S.E.M. (n≥3). HAD1 activity against sugar phosphates was previously described (Guggisberg,
772 Park, et al., 2014). Sugar phosphates (white bars) are ordered from left to right by increasing
773 number of carbon atoms (3-15). Nucleotides (black bars) are ordered from left to right by
774 increasing degree of phosphorylation. Abbreviations: Glc2P, glycerol 2-phosphate; Glc1P,
775 glycerol 1-phosphate; Gly3P, glyceraldehyde 3-phosphate; DHAP, dihydroxyacetone phosphate;
776 Glu1P, glucose 1-phosphate; PEP, phosphoenolpyruvate; 2-PGA, 2-phosphoglyceric acid; Ery4P,
777 erythrose 4-phosphate; Ribu5P, ribulose 5-phosphate; DOXP, deoxyxylulose 5-phosphate; Rib5P,
778 ribose 5-phosphate; 2drib5P, 2-deoxyribose 5-phosphate; MEP, methylerythritol phosphate;

779 Fru1P, fructose 1-phosphate; Man6P, mannose 6-phosphate; Glu6P, glucose 6-phoshpate; Fru6P,
780 fructose 6-phosphate; FBP, fructose 1,6-bisphosphate; Gal1P, galactose 1-phosphate; Sorb6P,
781 sorbitol 6-phosphate; Man1P, mannose 1-phosphate; Sedo7P, sedoheptulose 7-phosphate; Tre6P,
782 trehalose 6-phosphate; Pyr5P, pyridoxal 5'-monophosphate; GMP, guanosine 5'-
783 monophosphate; AMP, adenosine 5'-monophosphate; XMP, xanthosine 5'-monophosphate; IMP,
784 inosine 5'-monophosphate; CMP, cytidine 5'-monophosphate; dCMP, 2'-deoxycytidine 5'-
785 monophosphate; dGMP, 2'-deoxyguanosine 5'-monophosphate; TMP, thymidine 5'-
786 monophosphate; UMP, uridine 5'-monophosphate; dUMP 2'-deoxyuridine 5'-monophosphate;
787 ADP, adenosine 5'-diphosphate; TDP, thymidine 5'-diphosphate; UDP, uridine 5'-diphosphate;
788 CDP, cytidine 5'-diphosphate; GDP, guanosine 5'-diphosphate; CTP, cytidine 5'-triphosphate;
789 ATP, adenosine 5'-triphosphate.
790

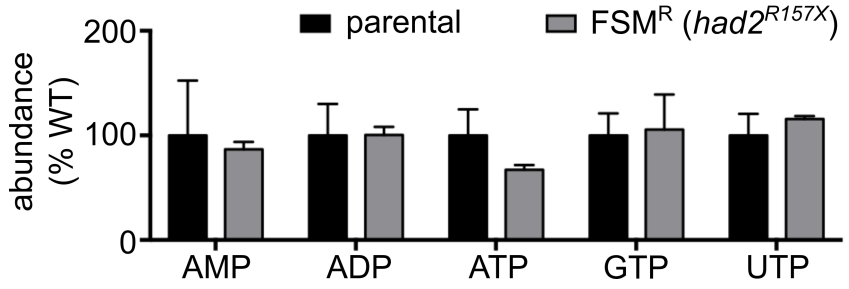

Figure 2-figure supplement 1. Nucleotide levels are unchanged in E2 FSM^R parasites. Error bars represent S.E.M. (n=3). A full panel of nucleotides was assessed. Of those detected, no metabolite is significantly changed in the FSM^R (*had2*^{R157X}) strain ($p>0.05$, unpaired Student's t-test). Other nucleotides were below the limit of detection.

798

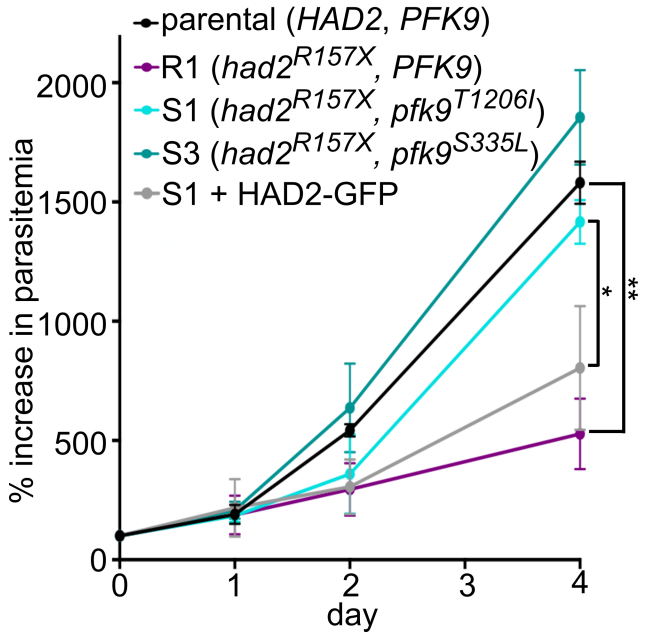

799

800 **Figure 3. FSM resistance results in a fitness cost.**

801 A representative FSM^{R} clone with the *had2*^{R157X} allele (R1, purple line) has a reduced growth

802 rate compared to the wild-type parental strain (black). The growth defect is rescued in two

803 representative clones with mutations in *PFK9* (S1 and S3, teal lines). Growth is normalized to

804 percent infected red blood cells on day 0. Error bars represent S.E.M. from independent growth

805 experiments ($n \geq 4$, ** = $p \leq 0.01$, * = $p \leq 0.05$, one-way ANOVA).

806

807

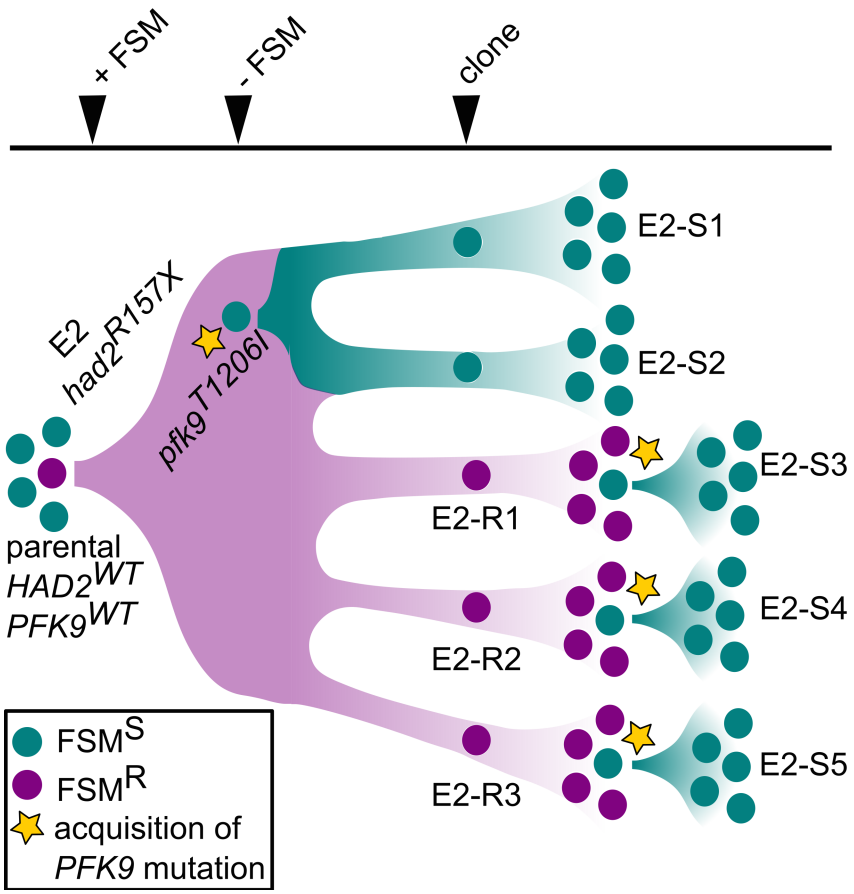

808

809 **Figure 4. Parasite selection scheme and genetic changes that modulate FSM sensitivity.**

810 Parasites are colored by their FSM phenotype (teal, FSM^S; purple, FSM^R). Cloned strains are

811 named by FSM phenotype (E2-SX, sensitive; E2-RX, resistant). A FSM^S parental strain was

812 selected under FSM pressure to enrich for FSM^R strain E2 (*had2*^{R157X}). After relief of FSM

813 pressure, a fitness advantage selects for spontaneous suppressor mutations in *PFK9* (*pfk9*^{mut},

814 yellow star) that result in FSM sensitivity. FSM^R clones are grown without FSM pressure and a

815 fitness advantage again selects for suppressor mutations in *PFK9* that result in increased growth

816 rate and loss of FSM resistance.

817

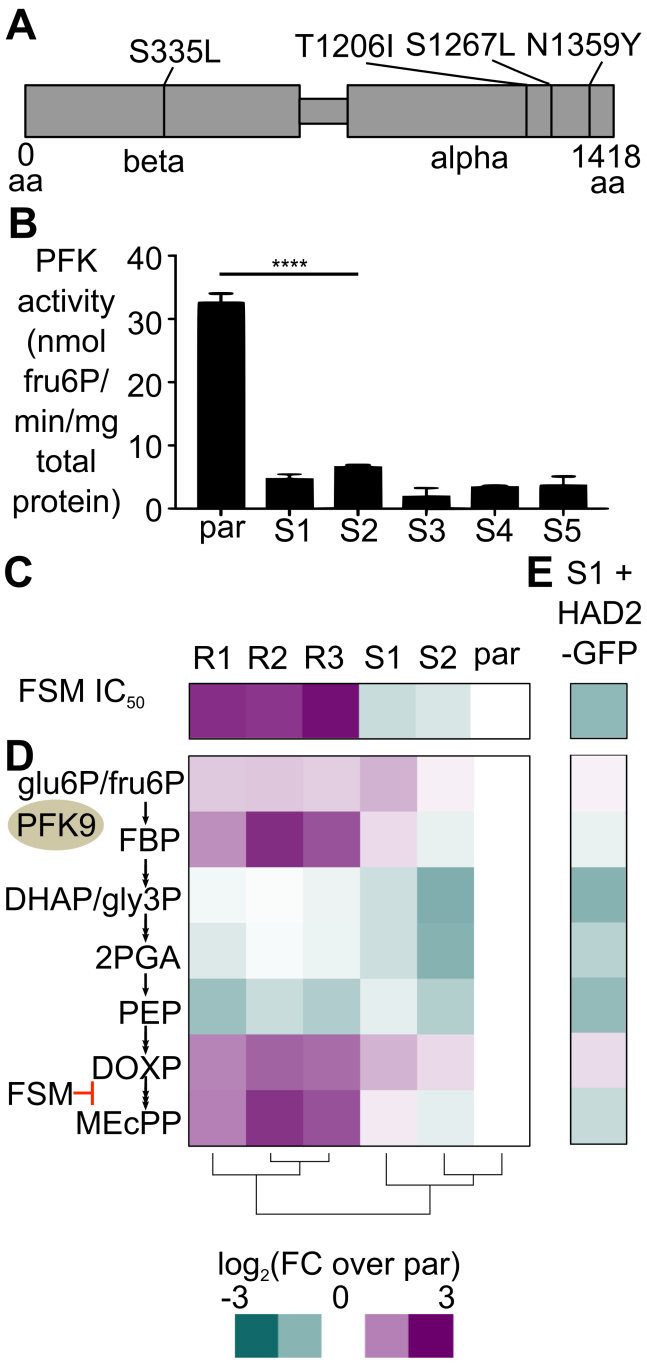

818

819 **Figure 5. *HAD2* and *PFK9* alleles alter FSM resistance, PFK activity, and metabolite levels**

820 **in *P. falciparum*.**

821 For heatmaps, colors represent the $\log_2$ of the fold change (FC) over the parental strain, as

822 indicated in the legend. Cloned strains are named by FSM phenotype (SX, sensitive; RX,

823 resistant). (**A**) Schematic of suppressor mutations identified in PFK9. Amino acid changes are
824 shown. (**B**) Measurement of PFK activity of *P. falciparum* lysate indicates that E2-SX clones
825 with *PFK9* suppressor mutations have significantly reduced PFK activity ($n \geq 3$, **** = $p \leq 0.0001$,
826 one-way ANOVA). Error bars represent S.E.M. Assay is linear and specific for PFK activity
827 (Figure 5-figure supplement 1). (**C**) FSM IC_{50}s for parental (par) strain and E2 clones. (**D**)
828 Metabolic profiling and clustering of parental and E2 clone strains demonstrates a metabolic
829 signature of resistance, which includes increased levels of MEP pathway intermediates DOXP
830 and MEcPP and the glycolytic metabolite FBP. Data are representative of at least three
831 independent experiments. Glu6P/fru6P and DHAP/gly3P represent isomer pairs that cannot be
832 confidently distinguished. Clustering performed using the heatmap function in R. (**E**) When loss
833 of HAD2 is rescued in $had2^{R157X}$, $pfk9^{T1206I}$ parasites, the resulting strain is hyper-sensitive to
834 FSM, due to functional HAD2 and a hypomorphic *PFK9* allele.
835
836

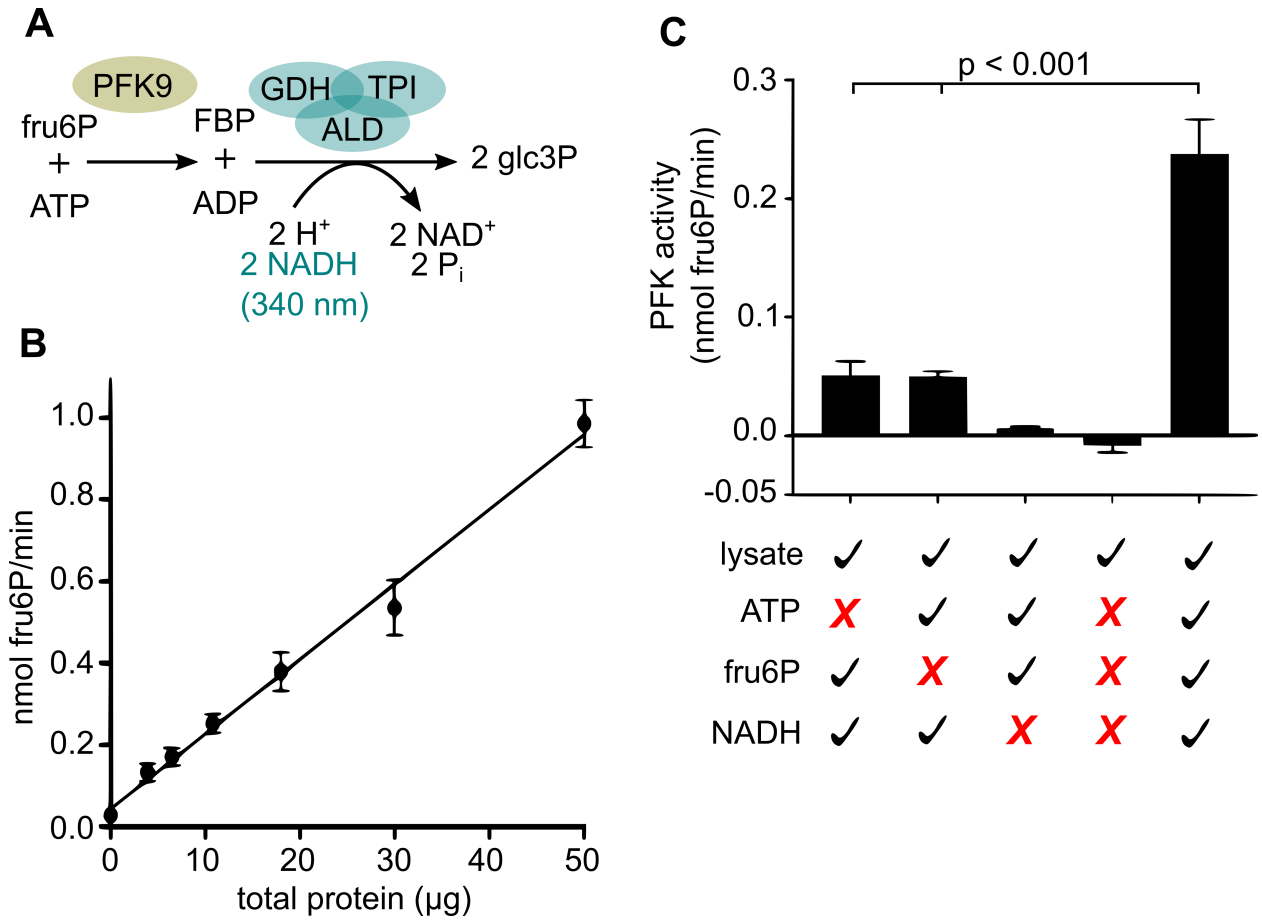

837

838 **Figure 5-figure supplement 1. Assay of PFK activity from *P. falciparum* lysate is linear and**

839 **specific.**

840 (**A**) Schematic of linked enzyme assay of PFK activity. PFK catalyzes the phosphorylation of

841 fructose 6-phosphate (fru6P) to fructose 1,6-bisphosphate (FBP). Excess linking enzymes

842 aldolase (ALD), triose-phosphate isomerase (TPI), and glycerol 3-phosphate dehydrogenase

843 (GDH) produce glycerol 3-phosphate. NADH utilization is monitored spectrophotometrically at

844 340 nm. (**B**) The assay is linear with respect to total lysate protein content. Error bars represent

845 S.E.M. (n=2). (**C**) The assay is specific for *P. falciparum* lysate-dependent PFK activity and

846 detects PFK activity above background (n=2, p<0.001). Error bars represent S.E.M.

847

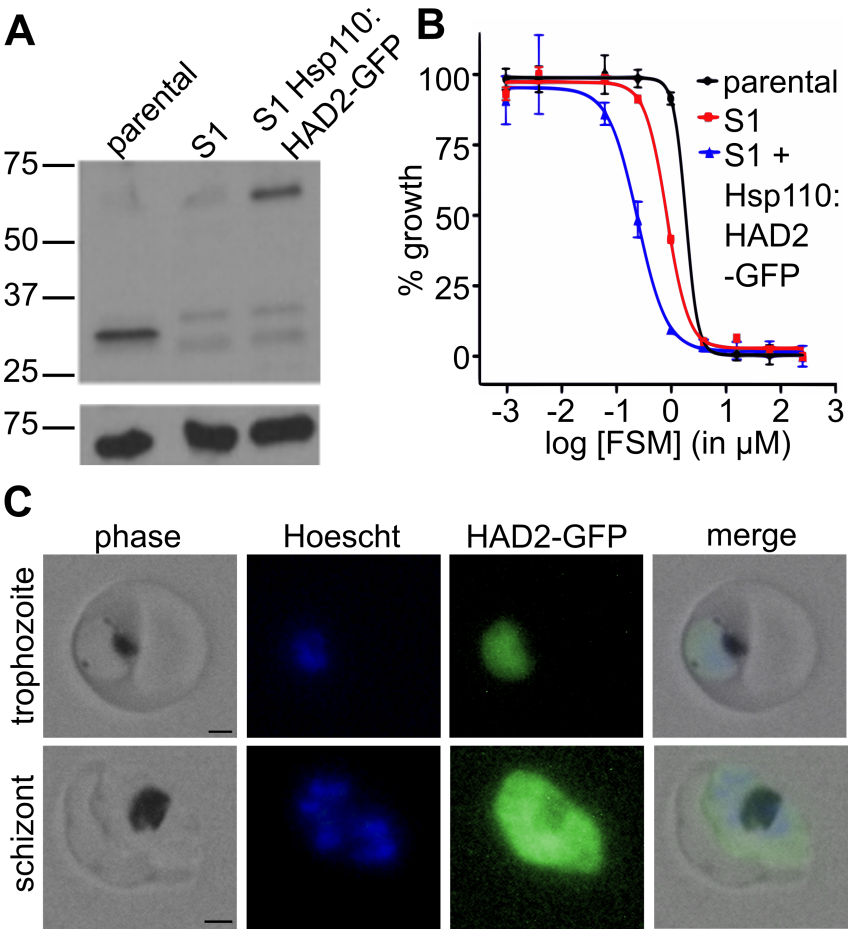

848

849 **Figure 5-figure supplement 2. Rescue of HAD2 confirms its role as a negative regulator.**

850 (**A**) Successful expression of pTEOE110:HAD2-GFP in strain S1 (*had2*^{R157X}, *pfk9*^{T1206I}) was

851 confirmed by immunoblot. Marker units are kilodaltons (kDa). Expected sizes: HAD2, 33 kDa;

852 HAD2-GFP, 60 kDa. The top blot was probed with anti-HAD2 antisera. The bottom blot was

853 probed with anti-heat shock protein 70 antisera as a loading control. Blot is representative of

854 three independent experiments. Minimal brightness adjustments were applied equally to all blot

855 images. (**B**) Representative FSM dose-response demonstrating expression of HAD2-GFP in

856 strain S1 (*had2*^{R157X}, *pfk9*^{T1206I}) results in oversensitivity to FSM. The parental strain has a FSM

857 IC_{50} of 0.8 ± 0.1 µM, and S1 has an IC_{50} of 0.5 ± 0.08 µM. When loss of HAD2 is rescued in

858 strain S1, the resulting strain has an IC_{50} of 0.3 ± 0.1 µM. Data shown are means and S.E.M. (n≥

859 3). (**C**) Live microscopy of E2 HAD2-GFP parasites indicates that HAD2-GFP localizes to the

860 parasite cytoplasm. Hoescht 33258 was used as a nuclear stain. Scale bars, 2 μm. Image

861 adjustments were applied equally to all images.

862

863

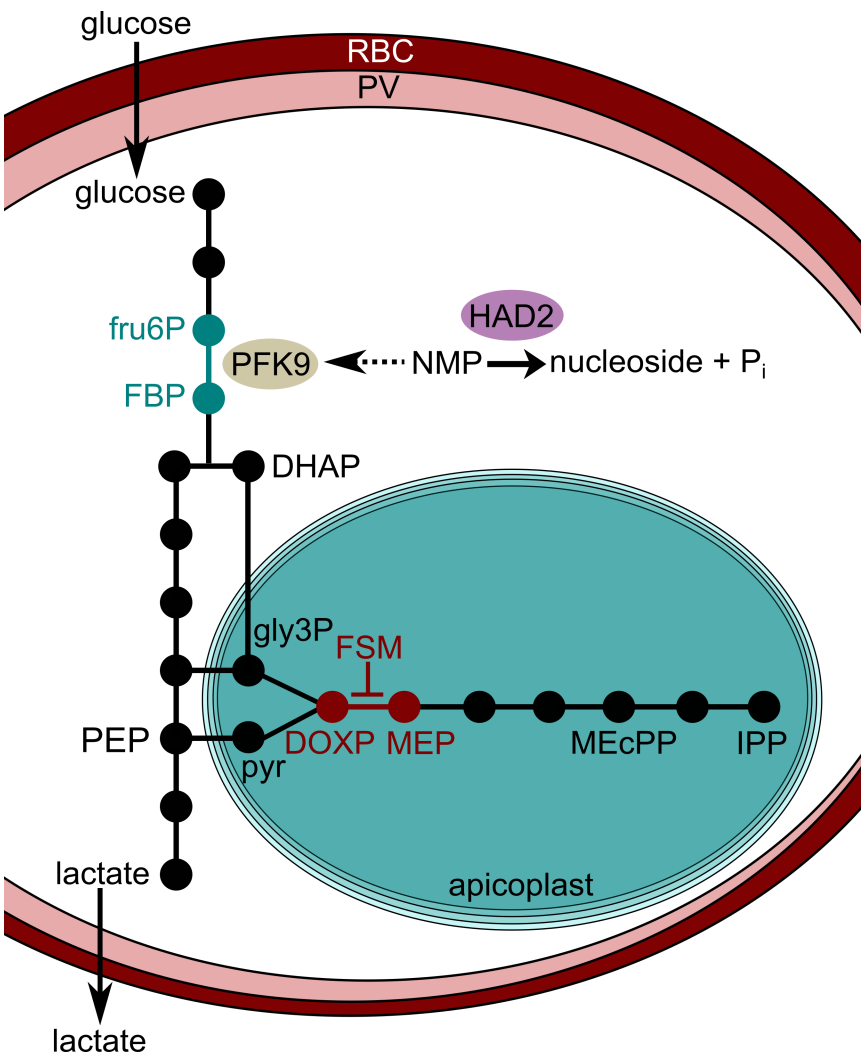

Figure 6. Model of HAD2-PFK9 metabolic regulation.

HAD2 may function as a negative glycolytic regulator at PFK9 by dephosphorylating nucleotides that function as positive allosteric regulators of PFK9. Loss of HAD2 results in increased flux through glycolysis and the MEP pathway, resulting in FSM resistance. Reduced PFK activity relieves this increased flux and restores FSM sensitivity. Abbreviations: RBC, red blood cell; PV, parasitophorous vacuole; NMP, nucleotide monophosphate.

874 **Table 1. Kinetic parameters for HAD2.**

875 Shown are the mean kinetic parameters for HAD2 against various substrates. Error bars represent
876 S.E.M. (n≥ 3). Abbreviations used: AMP, adenosine 5'-monophosphate; GMP, guanosine 5'-
877 monophosphate; 2dGMP, 2'-deoxyguanosine 5'-monophosphate; XMP, xanthosine 5'-
878 monophosphate; IMP, inosine 5'-monophosphate.

879

Substrate	K_m **(mM)**	K_{cat} **(sec^{-1})**	k_{cat}/K_m **(M^{-1} sec^{-1})**
AMP	1.0 ± 0.2	1.7 ± 0.3	1.7 x 10^3
GMP	0.30 ± 0.07	2.0 ± 0.1	6.9 x 10^3
2dGMP	0.30 ± 0.01	3.2 ± 0.5	11.0 x 10^3
XMP	0.73 ± 0.09	3.6 ± 0.1	5.0 x 10^3
IMP	8.4 ± 0.6	2.5 ± 0.1	0.30 x 10^3

880